A Framework for the Statistical Analysis of Large Radar and Lightning Datasets: Results from STEPS 2000

TIMOTHY J. LANG AND STEVEN A. RUTLEDGE

Department of Atmospheric Science, Colorado State University, Fort Collins, Colorado

(Manuscript received 30 September 2010, in final form 4 February 2011)

ABSTRACT

A framework for the statistical analysis of large radar and lightning datasets is described and implemented in order to analyze two research questions in atmospheric electricity: storms dominated by positive cloud-to-ground (+CG) lightning and estimating the probability of lightning in convection. The framework—a collection of computer programs running in series—is fully modular, allowing the analysis of a variety of datasets based on a study's objectives, including radar observations, lightning data, observations of meteorological environments, and other data. The framework has been applied to over 2 months of observations of 28 463 cells. The results suggest that +CG-dominated cells contain midlevel positive charge (−10° to −30°C), in contrast to cells dominated by −CG lightning, which typically had positive charge at upper (near −40°C) and lower levels (0° to −10°C). The +CG cells also were larger and more intense, and were associated with environments that were more convectively favorable—in terms of increased moisture, shear, and especially instability—when compared to −CG cells. The framework was also used to examine the probability of lightning occurrence for a spectrum of radar structures. The existence of 30-dBZ echo above the freezing altitude is a ''necessary'' condition (in ~90% of cases) for lightning occurrence. A ''sufficient'' condition (in ~90% of cases) is 40-dBZ echo breaching the freezing altitude. Altitude or volume of 40-dBZ echo was the superior estimator for the occurrence of lightning, while 30 dBZ was better for inferring the lack of lightning.

1. Introduction

a. On the need for a statistical framework to analyze large radar and lightning datasets

Currently, the U.S. national network of the Weather Surveillance Radar-1988 Doppler (WSR-88D) radars is being upgraded to polarimetric capabilities (Ryzhkov et al. 2005). This is coupled with both regional and global coverage of cloud-to-ground (CG) lightning provided via networks managed by various institutions (e.g., Lay et al. 2004; Cummins and Murphy 2009; Neilley and Bent 2009). There also exists a growing number of three-dimensional (3D) lightning mapping arrays in the United States, covering portions of several states. Finally, there is a plan to place lightning sensors on future geostationary satellites (Christian et al. 1989; Stuhlmann et al. 2005; Christian 2008). Collectively, these datasets represent a wealth of information for storm electrification research, particularly when coupled with existing datasets of atmospheric soundings, objective environmental (re)analyses, and satellite- and ground-mapped aerosol distributions.

However, the vast amount of data makes it imperative to process the information in an automated manner, as opposed to a case study approach. A major benefit of having truly national polarimetric and Doppler radar, lightning, environmental, and aerosol data will be the ability to examine regional differences in storm structure and electrification, and their potential relationships to environmental parameters and aerosol backgrounds. This is the promise of the forthcoming datasets, but automated analysis techniques will be required to fully exploit them.

Toward this end, a framework for the statistical analysis of radar, lightning, environmental, and aerosol data has been developed at Colorado State University (CSU). This framework, called the CSU Lightning, Environment, Aerosols, and Radar (CLEAR), is capable of incorporating a wide array of data sources and types. The capabilities of CLEAR will be demonstrated by examining two research problems in atmospheric electricity: storms dominated by positive CG (+CG) lightning and

Corresponding author address: Timothy J. Lang, 1371 Campus Delivery, Fort Collins, CO 80523.
E-mail: tlang@atmos.colostate.edu

DOI: 10.1175/MWR-D-10-05000.1

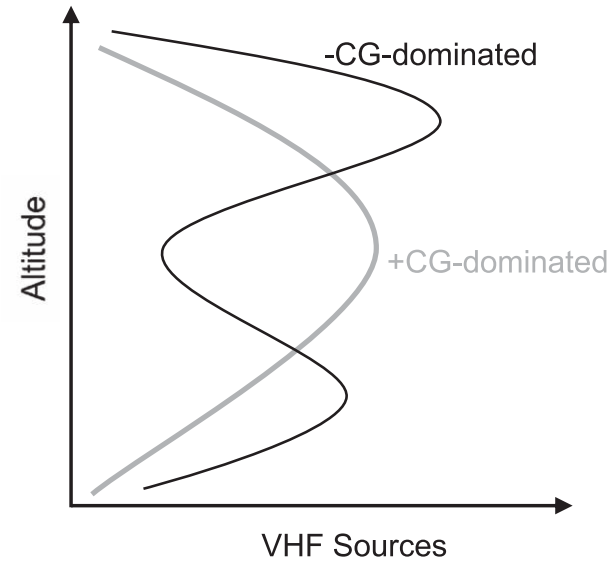

FIG. 1. Schematic illustration of typical VHF source density histograms by altitude, for idealized −CG-dominated storms (black) and +CG-dominated storms (gray) with approximately tripolar (either normal or inverted) charge structures.

estimating the probability of lightning given only radar observations.

b. *The problem of storms dominated by positive cloud-to-ground lightning*

While approximately 90% of CG lightning in the United States is negative in polarity (Orville and Huffines 2001), a class of storms exists that produces predominantly +CG lightning (Brook et al. 1982; Reap and MacGorman 1989; Engholm et al. 1990; Branick and Doswell 1992; Curran and Rust 1992; Seimon 1993; MacGorman and Burgess 1994; Stolzenburg 1994; Carey and Rutledge 1998; Smith et al. 2000; Williams 2001; Zajac and Rutledge 2001; Gilmore and Wicker 2002; Carey et al. 2003a,b; Carey and Rutledge 2003; Lang et al. 2004a; Wiens et al. 2005; Tessendorf et al. 2007a; MacGorman et al. 2008). These storms are typically intense, and in the United States are confined mainly to the Great Plains region. It is thought that +CG-dominated storms arise due to the presence of an inverted charge structure (Rust and MacGorman 2002; Lang et al. 2004a; Rust et al. 2005; Wiens et al. 2005; MacGorman et al. 2005, 2008; Tessendorf et al. 2007a); namely, positive charge in the middle levels of a thundercloud (−10° to −30°C) in place of the usual negative charge in this location (Williams 1989). The idealized charge structure that seems most favorable for +CG lightning is an inverted tripole, with a negative charge sandwiching the midlevel positive charge (Mansell et al. 2005; Wiens et al. 2005; Kuhlman et al. 2006; Tessendorf et al. 2007a; MacGorman et al. 2008). However, these observations have come only via case studies, and have not been verified with a large dataset.

It is useful to consider what idealized versions of −CG-dominated and +CG-dominated storms would resemble in data obtained from a 3D very-high-frequency (VHF) lightning mapping array. Assuming that a −CG storm typically would feature a normal polarity tripole structure (Williams 1989; Mansell et al. 2002; Tessendorf et al. 2007a), while a +CG storm would have an inverted tripole, and noting that negative leaders traveling through positive charge are inherently more noisy at VHF than are positive leaders in negative charge (Rison et al. 1999), then vertical histograms of VHF source density should resemble Fig. 1. The −CG storm would have positive charge at upper and lower levels, with negative charge in the midlevels. This corresponds to a bimodal structure in VHF source distribution in the vertical (Tessendorf et al. 2007a; Lang and Rutledge 2008). Meanwhile, the inverted +CG storm would have a single mode, near the midlevels where the positive charge dominates (Wiens et al. 2005; MacGorman et al. 2008).

A second question is how +CG storms become inverted. A leading hypothesis is graupel gaining positive charge during collisions with ice crystals in the presence of supercooled liquid water (Wiens et al. 2005; Williams et al. 2005; Carey and Buffalo 2007; MacGorman et al. 2008). This is most likely to occur in large liquid water contents, which can flip the sign of charge deposited on graupel (from the usual negative) at a given temperature (Takahashi 1978; Saunders et al. 1991; Saunders and Peck 1998). These superlative water contents are consistent with the presence of strong, broad updrafts (implying a larger storm; Lang and Rutledge 2002), which commonly occur in certain meteorological environments (Williams et al. 2005; Carey and Buffalo 2007). In particular, increased values of instability, shear, and cloud-base height (leading to reduced warm-cloud depth) could encourage the development of strong broad updrafts with high liquid water contents in the mixed-phase zone of a cloud (0° to −40°C; Williams et al. 2005; Lang and Rutledge 2006; Carey and Buffalo 2007). According to this hypothesis, compared to −CG storms, +CG storms are expected to develop in more unstable and sheared environments, should feature reduced warm-cloud depths (Williams et al. 2005; Carey and Buffalo 2007), and be larger overall (Lang and Rutledge 2002; Wiens et al. 2005; Tessendorf et al. 2007a).

c. *The problem of inferring lightning with radar data*

There is a long history of analyzing the relationships between conventional radar reflectivity, storm electrification,

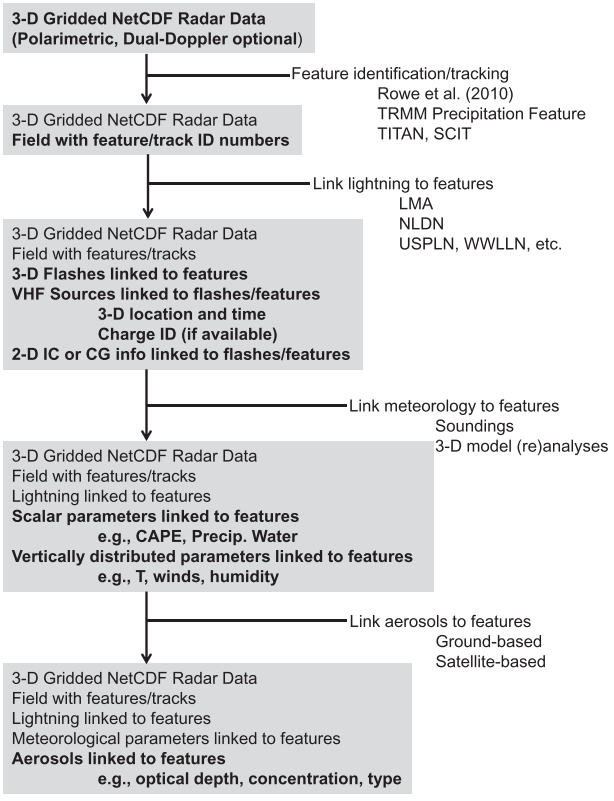

FIG. 2. Schematic depiction of CLEAR. The aerosol functionality was not used in this study.

and lightning. These studies include, but are not limited to, Workman and Reynolds (1949), Larsen and Stansbury (1974), Marshall and Radhakant (1978), Dye et al. (1989), Buechler and Goodman (1990), Michimoto (1991, 1993), Petersen et al. (1996), Gremillion and Orville (1999), Vincent et al. (2003), Wolf (2007), and Stano et al. (2010). The general scope of the results is that the existence of +40-dBZ echo at or above the altitude of −10°C corresponds to a very high probability of lightning. The existence of 30 dBZ in the mixed-phase region appears to be the minimum for a storm to have any possibility of producing lightning.

However, these studies typically focused only on CG lightning, and did not use total lightning data. Since intracloud (IC) lightning typically precedes CG lightning (Larsen and Stansbury 1974; Goodman et al. 1988; MacGorman et al. 1989; Carey and Rutledge 1996), radar criteria might be different if total lightning were considered instead. In addition, these studies were focused on predicting lightning, and hence there was considerable effort applied toward maximizing lead time and skill scores, rather than just asking the simple question: given an observed radar structure, what is the probability of lightning currently occurring in a storm? Though answering this question has applications in lightning warning and prediction, perhaps the strongest application would be in forensic meteorology, for example in the study of (potentially) weather-related aviation accidents, where the question is often whether a cloud was producing lightning (often undetected IC lightning) at the time of an accident—implying dangerous turbulence. Thus, there is a need for a broad-based analysis—using total lightning data—to examine the probability of lightning's existence over a spectrum of radar-observed storm structures.

2. Data and methodology

a. Overview

The data for this study come from the Severe Thunderstorm Electrification and Precipitation Study (STEPS), which took place in eastern Colorado and western Kansas during the summer of 2000 (Lang et al. 2004a). Operational radar data and research lightning network data were available for nearly all of 25 May through 10 August. The present study focused on this time period, and thus both encompassed and expanded upon the multitude of STEPS case studies that have appeared in the literature (Lang and Rutledge 2002; Rust and MacGorman 2002; Lyons et al. 2003a,b; Warner et al. 2003; Lang et al. 2004a,b; MacGorman et al. 2005; Rust et al. 2005; Tessendorf et al. 2005; Wiens et al. 2005, Kuhlman et al. 2006; Tessendorf et al. 2007a,b; Deierling et al. 2008; Deierling and Petersen 2008; Krehbiel et al. 2008; Lang and Rutledge 2008; Lyons et al. 2008; Weiss et al. 2008).

b. Basic concept of CLEAR

Before addressing how data from each STEPS platform was analyzed, it is important to delineate the basic features of CLEAR. CLEAR is a collection of computer programs that work in series to efficiently merge and analyze large amounts of radar, environmental, CG lightning detection network, and 3D lightning mapping, and other data (Fig. 2). CLEAR was written in the Interactive Data Language (IDL), and is automated so that large amounts of data can be ingested, yielding various types of synthesized results, which can reveal relationships between storm kinematics, microphysics, lightning, and environmental parameters such as convective available potential energy (CAPE), shear, and warm-cloud depth.

Initially, radar features (e.g., convective cells) are identified for each radar volume. The identified features are then associated with lightning data. Environmental data are taken from either soundings or model (re)analyses,

which can be analyzed to create a preconvective environmental sounding for each storm. In this way, the kinematic, microphysical, and lightning fields can be related to prestorm sounding parameters. Though not done in this study, CLEAR also can assimilate aerosol data from satellite and ground-based observations. Indeed, basic algorithms exist to input any sort of data relevant to storm research.

All data are stored in individual Network Common Data Form (NetCDF) radar volume files with tags linking radar features to their respective lightning, environmental, and other data. In other words, any specific radar feature (i.e., convective cell) can be linked to all radar observables associated with it (e.g., 3D reflectivity), all the lightning that occurred within it (locations of individual lightning mapping sources are stored), and the meteorological environment in which it existed. This additional information minimally increases file size (by ~10%–20%) for the traditional gridded radar NetCDF file, making CLEAR an efficient way to combine complex datasets. CLEAR is fully modular, so that different methodologies can be explored to ensure robust results.

c. General approach of this study

This study included the analysis of over two months of radar, lightning, and environmental data. The basic philosophical approach was to examine the two specific research problems, +CG storms and lightning probability, by examining contemporaneous relationships between radar-observed storm structure, lightning, and meteorological environment. Storms were analyzed on the basis of what they were doing during a particular radar volume scan, not what they did several minutes before or what they did over their lifetime. The results of Wiens et al. (2005) and other STEPS case studies clearly argue for comparing contemporaneous radar and lightning data. Moreover, the life cycles of individual convective elements (often 30 min or less) is well below the temporal resolution of the environmental analyses used in this study (1 h). Therefore, lag-based analyses with environmental data have no obvious benefits. Moreover, if a storm produced −CG lightning for a while but then switched over to +CGs (Smith et al. 2000), the present study easily bypassed the question of how to label the storm by effectively treating those different times separately. Results may be sensitive to specific analysis choices, so sensitivity tests were performed to address this concern.

d. KGLD WSR-88D radar

1) Data details and grid creation

Goodland, Kansas (KGLD), WSR-88D radar data were obtained in level-II format from the National Climatic Data Center (NCDC; http://www.ncdc.noaa.gov). Essentially 24-h coverage, with updates every 5–6 min based on scan type, was available for the analysis period, except for two missing days: 8–9 July 2000. The reflectivity field from every volume was interpolated to a 2 km × 2 km (horizontal) × 1 km (vertical) Cartesian grid using the National Center for Atmospheric Research (NCAR) Reorder software package (see online at http://www.eol.ucar.edu/rdp/home/reorder.html). A Cressman (1959) filter with a 1° elevation and azimuth radius of influence was used during this process. This grid is coarse, but it is consistent with the resolution provided by normal WSR-88D scan patterns. Manual inspection of select volumes ensured that gridding worked well with minimal artifacts. This approach to WSR-88D data was nearly identical to those employed by Lang and Rutledge (2008) and Lang et al. (2010). The grid was centered on the KGLD radar and spanned the region −174 to 126 km east and −150 to 150 km north, as well as 1.5 to 20.5 km above mean sea level (MSL). For reference, KGLD radar elevation was 1.1 km MSL. While two polarimetric radars were available during STEPS (Lang et al. 2004a), they lacked the long-term, wide-angle viewing provided by KGLD.

2) Feature identification

Radar feature identification was accomplished via a variant of the method of Rowe et al. (2011), who described a cell-tracking algorithm used on a two-dimensional (2D) gridded radar field (in this case maximum reflectivity in a vertical column). The algorithm is based in part on the Thunderstorm Identification, Tracking, Analysis, and Nowcasting (TITAN) program (Dixon and Wiener 1993), which automatically identifies reflectivity centroids typically associated with convective cells. Another key aspect of the Rowe et al. (2011) methodology is the use of two reflectivity thresholds to identify features. The use of multiple thresholds is available in the Storm Cell Identification and Tracking (SCIT) algorithm (Johnson et al. 1998), and has been shown to improve the identification of individual convective elements, like those within a mesoscale convective system (MCS). While Rowe et al. (2011) used 35- and 45-dBZ thresholds, in this study 30 and 45 dBZ were chosen after testing. Most threshold choices worked well on isolated convection, but it was found, subjectively, that 30 and 45 dBZ provided the best separation of individual cells in STEPS multicell storms, such as the 11–12 June 2000 system studied by Lang et al. (2004b) and Lang and Rutledge (2008). The minimum areas used to identify a cell were 16 km^2 for the 30-dBZ threshold (4 pixels) and 8 km^2 for 45 dBZ (2 pixels). These values eliminated noisy pixels from being considered as radar features in the coarse STEPS grids. All cells

are considered whether they were isolated, or part of a multicellular storm such as an MCS (these typically contained many individual radar features per volume, and were not considered a single feature).

For various computations (e.g., echo-top height, volume contained within a feature, etc.), features were expanded to 3D by examining all of the echo in the vertical columns contained within the 2D area identified as a feature. For example, if a feature consisted of five 2D pixels, the vertical columns associated with those pixels were analyzed. Gauthier et al. (2010) used a variant of this software in their radar and lightning analysis.

e. STEPS LMA

Technical details of the STEPS lightning mapping array (LMA), and the basic methodology of analyzing its data, have been reviewed in the past (e.g., Lang et al. 2004a; Thomas et al. 2004; Wiens et al. 2005). Therefore, only details relevant for the present study will be discussed here.

The processing and analysis of full-rate LMA data are extremely computational resource intensive. Therefore, only decimated LMA data were used in this study. Decimation involves using only the highest-power VHF source in a longer time period than the native resolution of LMAs (~50 ns), in a given location. The decimation applied to the STEPS dataset reduced LMA sources by about 80%. This required some compromises: because of the reduced number of data points, flash counting was not attempted. Individual LMA sources were linked to a radar feature if they occurred within the feature or if it was the closest feature within 10 km. Since LMA-mapped lightning is strongly tied to individual convective cores, even in MCSs (e.g., Lang and Rutledge 2008), changing this threshold did not affect results.

Wiens et al. (2005) demonstrated that rate of occurrence of sources is well correlated with LMA-derived flash rates, so even without flash data basic information about electrical activity was maintained. In addition, most STEPS studies involving LMA analysis have used source densities to identify the most electrically active portions of storms (e.g., Wiens et al. 2005; Lang and Rutledge 2008; Weiss et al. 2008). Indeed, one of the principal questions of this study was the following: were +CG-dominated STEPS storms more electrically active than −CG-dominated ones? Also, were there differences in the vertical distribution of VHF sources between +CG- and −CG-dominated storms? Questions like these are answerable using decimated sources.

VHF sources were required to have been detected by ≥7 LMA stations, and to have a chi-squared value ≤1, similar to Lang and Rutledge (2008) and Lang et al. (2010). This eliminated most noisy sources. Only radar features whose reflectivity centroid fell within 125 km of the LMA network's centroid were included in this study's analyses. This range gave approximately 1 km or better vertical resolution of LMA sources (Lang et al. 2004a; Thomas et al. 2004). While 13 LMA stations were available during STEPS, not every station was operational the entire time. Indeed, less than 9 stations were available during portions of mid-July. Data from these periods were eliminated by requiring at least 9 stations to be active; otherwise' some storms could have had artificially reduced source counts due to the 7-station detection requirement. LMA data from periods of absolutely no electrical activity, as well as from some corrupted files, were not included as these data files were unreadable by xlma. This amounted to ~50% of the entire 25 May–10 August 2000 period, but this almost exclusively was during convective minima such as mornings, when few if any radar features were identified.

f. NLDN

This study used 1-ms resolution NLDN stroke data, similar to Lang et al. (2004a,b), Wiens et al. (2005), Tessendorf et al. (2007a,b), and Lang and Rutledge (2008). Also like these studies, +CGs with peak currents under 10 kA were not counted, per the pre-2002 upgrade recommendations of Cummins et al. (1998). Narrow bipolar events misclassified as +CGs by the NLDN were not inferred (Tessendorf et al. 2007a). The CG strokes were linked to a radar feature if they struck within its boundaries or if it was the closest feature within 10 km. Changing this threshold did not affect results as the latter criterion encompassed a very small percentage of strokes.

g. RUC hourly isobaric analyses

Hourly analyses from the Rapid Update Cycle (RUC) model (Benjamin et al. 2004a,b) were used in this study. The analyses were isobaric and available at 40-km resolution. They contained a number of vertically distributed variables such as temperature T, as well as 2D variables like CAPE. When presented with a radar feature at a given time and location, the first task was to linearly interpolate all the data from two successive RUC files to match the start time of the radar feature's volume scan. The 2300 UTC file was not available for most days, so for features occurring between 2200 and 0000 UTC these respective RUC analyses were used for interpolation over a 2-h period instead.

Then, the closest grid point in space to the radar feature was identified in the temporally interpolated RUC data. The RUC analyses estimated storm motion for every grid point, so the storm motion vector was used to

determine the next closest grid point that would be in the direction of a feature's travel. It was this latter grid point from which environmental data were extracted and associated with the radar feature in its NetCDF file. This was an attempt to sample the environment into which the radar feature was moving.

This study's settings for proximity soundings fit within the so-called Goldilocks Zone for optimum spacing and timing of storm-environment soundings (40–80 km, 0–2 h) advocated by Potvin et al. (2010). That study argued that soundings too close to storms could be influenced by convection, while those too far away would be unrepresentative. Though discussed in more detail in section 3e, sensitivity studies showed that simply using the nearest RUC gridpoint neighbor of a radar feature produced very similar results to the more complex method described above.

Most environmental data were provided directly by the RUC analyses. However, some were calculated using the wind, temperature, and moisture parameters provided by the RUC. These included cloud-base height, which was estimated from surface (2 m) temperature and dewpoint via the methodology of Williams et al. (2005), and parameters derived from cloud-base height such as warm-cloud depth. The 3- and 6-km shear and bulk Richardson number were calculated using the RUC-provided wind fields, and lapse rates in various layers were derived from RUC temperatures.

Thompson et al. (2003) evaluated RUC analysis-derived proximity soundings, and found them to be very accurate, although near the near the surface temperatures were too cool by about 0.5°C, with an overestimate of wind speeds of about 1–2 m s^{-1}, compared to radiosonde measurements. CAPE was underestimated by 0–250 J kg^{-1}, while shear estimates were accurate. Thompson et al. (2003) noted that the magnitudes of these errors were similar to errors commonly associated with radiosonde measurements, and argued that RUC soundings were a ''reasonable proxy'' for real soundings. Both Hane et al. (2008) and Kalb (2007) also performed intercomparisons of RUC data with individual soundings, and obtained results similar to Thompson et al. (2003). Because of this success, there have been a number of studies throughout the past decade that used proximity soundings based on RUC output to study storm environments (e.g., Markowski et al. 2003; Schumacher and Johnson 2005; Hane et al. 2008).

Finally, absolute accuracy was less important in this study as it was focused on relative differences between storm types (e.g., the different environments of +CG and −CG storms). Therefore, the superior spatial and temporal coverage of the RUC data outweighed any possible concerns about its accuracy.

3. Results

a. Overview

There were 28 463 features identified over the course of the analysis period. Of this number, 1561 produced at least 1 +CG stroke and at least as many +CG strokes as −CG strokes during the radar volume containing each feature (i.e., ≥50% positive). These were labeled +CG-dominated features (or +CG features for short). Similarly, 3329 features produced at least 1 −CG stroke and had more −CG strokes than +CG strokes during each feature's radar volume. Such features were labeled −CG-dominated features (or −CG features). There were 23 573 features that produced no CGs of either polarity. These features were split into two types: those with no CG lightning, but still producing VHF sources as detected by the LMA (7900 no-CG features), and those producing no VHF sources (15 673 no-lightning features).

Thus, only a small percentage of the radar features produced CGs of any type (17.2%), while a clear majority of features (55.1%) produced no lightning whatsoever. Indeed, despite the association of the STEPS region with +CG storms (Lang et al. 2004a), +CG-dominated features were a small minority (5.5%) of all features, and were outnumbered by −CG-dominated features by over 2:1. The major +CG outbreaks, by UTC-defined day, were on 20 July (211 +CG features), 22 July (180), and 23 June (126), together accounting for about a third of all +CG features during STEPS. Interestingly, these days did not include the best-known +CG case days from STEPS, such as 29–30 June (Lang and Rutledge 2002; Warner et al. 2003; Lang et al. 2004a; MacGorman et al. 2005; Tessendorf et al. 2005; Wiens et al. 2005; Kuhlman et al. 2006; Lyons et al. 2008). But +CG storm days were not rare, as 29 of 78 days included at least 10 observed +CG features apiece (29–30 June were among these active +CG days).

b. +CG versus −CG features

While collectively a small percentage of all features, there were enough +CG and −CG features to obtain robust statistics of their basic lightning behavior, radar structures, and meteorological environments. Table 1 lists the key results of this comparison, while Table 2 lists the statistical significance of the observed differences. The +CG features were more electrically active than −CG features, by a factor greater than 3:1. The +CG features also were significantly larger than their −CG counterparts, with taller echo-top heights and far more 30- and 40-dBZ echo volume above the freezing altitude.

The biggest environmental difference between the two types was that +CG features were associated with nearly twice as much CAPE, on average. The increased

TABLE 1. Comparison of mean values for parameters associated with +CG, −CG, no CG, and no-lightning radar features. The AGL was approximately 1.1 km MSL. See text for other acronym definitions.

	+CG	−CG	No CG	No lightning
No. of features	1561	3329	7900	15 673
VHF source rate (min^{-1})	2620.0	811.1	206.8	0.0
+CG rate (min^{-1})	1.0	0.1	0.0	0.0
−CG rate (min^{-1})	0.2	1.5	0.0	0.0
CAPE ($J\ kg^{-1}$)	1603.0	904.3	1264.2	950.8
CIN ($J\ kg^{-1}$)	−65.5	−81.4	−64.3	−78.9
Lifted index	−4.2	−2.9	−3.4	−2.8
850–500-hPa lapse rate ($K\ km^{-1}$)	−7.4	−7.3	−7.5	−7.2
700–500-hPa lapse rate ($K\ km^{-1}$)	−7.9	−8.0	−7.9	−7.8
Cloud-base height (km AGL)	1.28	1.35	1.48	1.20
Freezing-level altitude (km AGL)	3.54	3.47	3.52	3.48
Warm-cloud depth (km)	2.25	2.11	2.04	2.27
0–3-km shear ($m\ s^{-1}$)	10.7	9.3	9.4	9.8
0–6-km shear ($m\ s^{-1}$)	17.9	15.8	15.8	16.6
Bulk Richardson number	32.1	13.0	54.5	15.8
Storm-relative helicity ($m^2\ s^{-2}$)	136.6	112.3	114.4	91.3
Equilibrium level (km MSL)	12.0	10.8	11.3	10.4
Precipitable water (mm)	26.4	24.8	25.4	24.8
Equivalent potential T (K)	309.1	310.5	310.5	308.3
2-m T (°C)	24.0	23.6	24.8	22.7
2-m dewpoint (°C)	13.3	12.3	12.5	12.7
0-dBZ echo-top height (km MSL)	15.8	14.5	13.5	9.5
30-dBZ echo-top height (km MSL)	12.3	10.5	8.7	4.9
40-dBZ echo-top height (km MSL)	10.0	7.6	5.3	1.4
0-dBZ volume ($10^3\ km^3$)	16.510	9.342	2.861	0.641
30-dBZ volume $T < 0$°C ($10^3\ km^3$)	4.060	1.627	0.466	0.042
40-dBZ volume $T < 0$°C ($10^3\ km^3$)	1.468	0.409	0.110	0.002

instability associated with +CG features also showed in the numbers for lifted index and convective inhibition (CIN), although results for lapse rates in different layers were mixed. The +CG features also were associated with increased wind shear and storm-relative helicity. Bulk Richardson numbers were larger for +CG features, driven by the large differences in CAPE, but smaller shear variability between feature types. Equilibrium levels were over 1 km taller for +CG features on average, consistent with the ~1-km mean difference in 0-dBZ echo-top heights. The observed discrepancies between echo-top heights and equilibrium levels suggest that the RUC may have been underestimating the latter, but also could include the effects of overshooting tops in intense features. One unexpected result, based on past studies (Williams et al. 2005; Lang and Rutledge 2006; Carey and Buffalo 2007), was that +CG features were associated with slightly lower cloud bases, leading to warm-cloud depths that were ~140 m deeper than −CG features.

While mean differences between feature types could be large, there were no obvious threshold values for environmental or radar variables beyond which solely +CG features would be observed. Figure 3 shows cumulative distribution functions for CAPE and 40-dBZ echo volume. At or above a given value for these parameters, proportionately more +CG features than −CG features existed, but −CG features could still be associated with high CAPE or large echo volumes. However, as environments became more conducive to intense convection, features grew larger and became more likely to produce predominantly +CG lightning during STEPS.

The +CG features also appeared to have different charge structures, compared to −CG features. Figure 4 shows a histogram of the vertical distribution of VHF sources by feature type. While not exactly matching the idealized model shown in Fig. 1, +CG features did have a unimodal distribution of sources, with a peak in the middle levels (8–9 km MSL; near −30°C), while the −CG source distribution peaked at a higher altitude (9–10 km; near −40°C), with a secondary hump at lower levels (5–6 km; near −10°C). To examine the effect of LMA sensitivity on this plot, Fig. 5 was developed, which repeated this analysis but only for radar features within 60 km of the LMA centroid. The lower positive charge center was much more apparent for −CG features—an actual relative maximum in LMA sources rather than a hump. It appears possible that closer features were better resolved by the LMA, allowing the lightning associated with the lower positive charge layer in −CG

TABLE 2. Statistical significance levels (in %) for differences between the means presented in Table 1 (based on a two-sided rank-sum test; Walpole et al. 2002). CG rate results are not shown since these were defining criteria for all categories.

	+CG vs −CG	+CG vs no CG	+CG vs no lightning	−CG vs no CG	−CG vs no lightning	No CG vs no lightning
VHF source rate	99	99	99	99	99	99
CAPE	99	99	99	99	99	99
CIN	99	97	68	99	99	99
Lifted index	99	99	99	99	99	99
850–500-hPa lapse rate	99	99	99	99	99	99
700–500-hPa lapse rate	99	87	99	99	99	99
Cloud-base height	82	99	99	99	99	99
Freezing-level altitude	99	82	99	99	99	99
Warm-cloud depth	99	99	53	99	99	99
0–3-km shear	99	99	99	40	99	99
0–6-km shear	99	99	99	57	99	99
Bulk Richardson number	99	99	99	99	99	99
Storm-relative helicity	99	99	99	51	99	99
Equilibrium level	99	99	99	99	99	99
Precipitable water	99	99	99	99	99	99
Equivalent potential T	99	99	99	90	99	99
2-m T	99	99	99	99	99	99
2-m dewpoint	99	99	99	49	85	53
0-dBZ echo-top height	99	99	99	99	99	99
30-dBZ echo-top height	99	99	99	99	99	99
40-dBZ echo-top height	99	99	99	99	99	99
0-dBZ volume	99	99	99	99	99	99
30-dBZ volume $T < 0$°C	99	99	99	99	99	99
40-dBZ volume $T < 0$°C	99	99	99	99	99	99

features to be more visible. However, only 7397 features fit this figure's criteria, with all but 1000 of them not producing any CGs, so this interpretation should be made with caution.

The differences in source altitudes were also apparent when analyzing source distribution mode versus CG flash rate (Fig. 6, which goes back to including all features within 125 km). As −CG stroke rate increased,

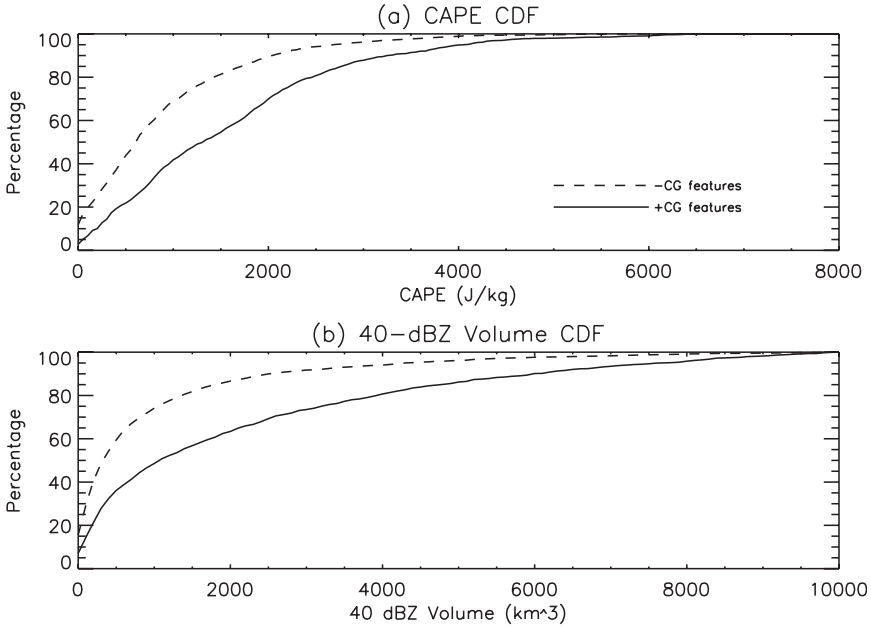

FIG. 3. Cumulative distribution functions (CDFs) of (a) CAPE and (b) volume of ≥40-dBZ radar echo, broken down by feature type.

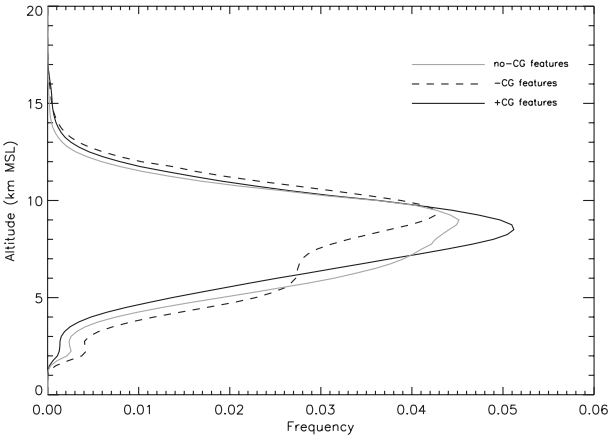

FIG. 4. Normalized vertical distributions of VHF sources, broken down by feature type.

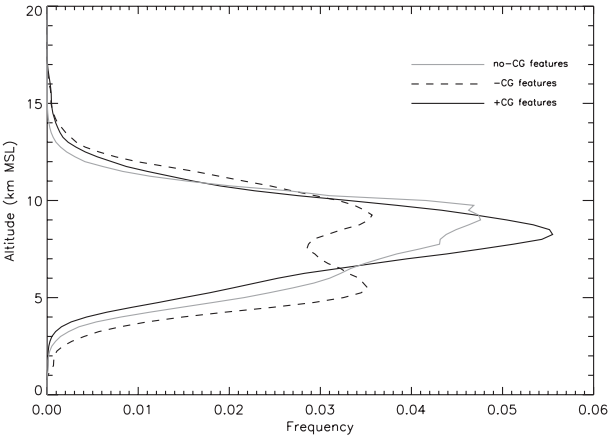

FIG. 5. As in Fig. 4, but only for features within 60 km of the LMA centroid.

features were more likely to have their maximum number of sources located either at high altitudes near 10 km MSL, or at low altitudes near 5–6 km, consistent with the existence of positive charge near either of these regions. Meanwhile, as +CG stroke rate increased, the source maximum was in the middle levels near 8 km, suggesting positive charge near there.

c. *Features producing no CG lightning*

While this study was focused on +CG and −CG features, it is important to understand their context by examining no-CG features. There were 7900 features that produced intracloud activity but no NLDN-detected CG lightning of either polarity (Table 1). These features generally populated active thunderstorm days that had lightning of all types, so it was reasonable to expect their meteorological environments to be a mix of those associated with +CG and −CG features. For example, based on inspection of the dataset, many no-CG features were related to early or late periods in storm cycles, and not the mature phase of storms when CG lightning was produced. As expected, most meteorological parameters fell between those associated with +CG and −CG features (Table 1). One notable exception, however, was cloud-base height [1.48 km above ground level (AGL)], which was 100–200 m higher than either of the CG-producing features. This was related to the slightly warmer surface temperatures that increased the surface dewpoint depression.

Overall, the reflectivity structure associated with no-CG features was significantly weaker than CG-producing ones (Table 1). They also had much smaller VHF source rates, which supported the inference of no-CG features as weaker portions of thunderstorm life cycles. No-CG features also likely included many marginal thunderstorms that perhaps produced a few IC flashes at peak, but never any CGs. Very few of these features were like the intense yet low-CG storms studied by other researchers (MacGorman et al. 1989; Lang et al. 2000; Lang and Rutledge 2002; McCaul et al. 2002). Indeed, the statistical evidence in Table 1 suggests that the intense no-CG storm studied by Tessendorf et al. (2007b) was anomalous for this region.

The vertical distribution of sources in no-CG storms appeared to reflect a combination of inverted and normal-polarity structures in individual features (Fig. 4). The peak altitude (9 km MSL) lay between that of −CG and +CG features, while in the lower levels the distribution was broader than that of +CG features but was not consistent with the existence of lower positive charge, as in −CG features.

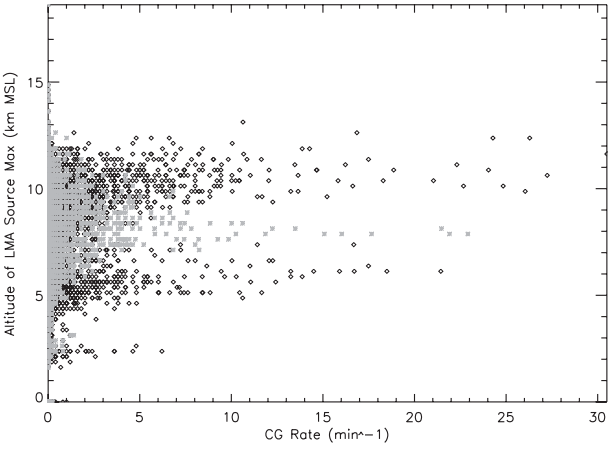

FIG. 6. Altitude of the mode of each feature's vertical distribution of VHF sources, plotted against its CG stroke rate (broken down by polarity).

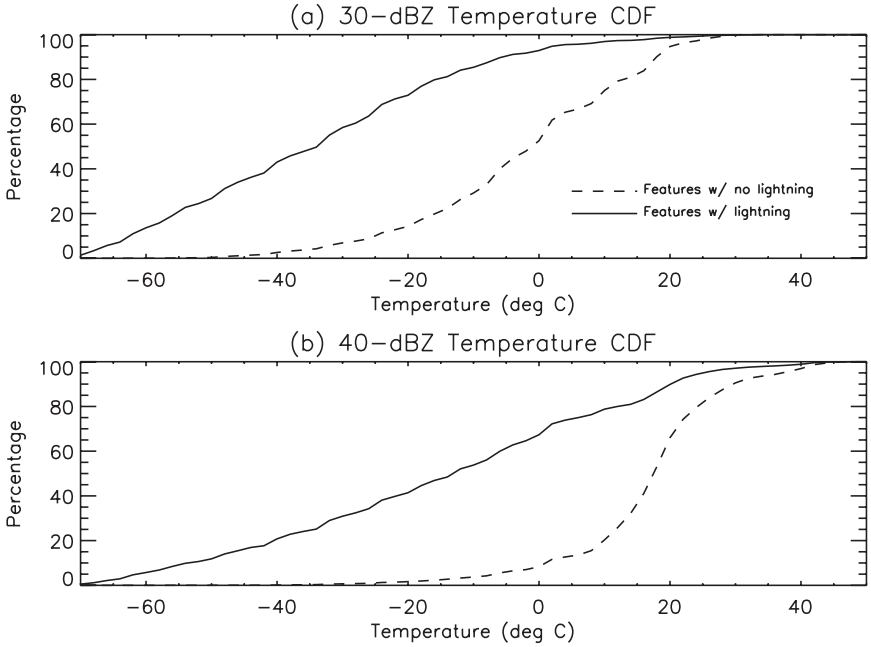

FIG. 7. CDFs of maximum height as a function of temperature for the (a) 30- and (b) 40-dBZ reflectivity contours, broken down by feature type.

d. Features producing lightning versus those with no lightning

The final topic of this study was examining differences between features producing lightning and those producing no lightning. There were 15 763 features that produced no lightning of any type (i.e., VHF source rate and CG rate were all 0), compared to 12 790 that produced at least some lightning (Table 1). No-lightning features likely composed weaker portions of a thunderstorm life cycles, or were just marginal, unelectrified convective cells. Their associated meteorological parameters sometimes fell between those of electrified features (e.g., CAPE), and sometimes were weaker altogether (e.g., lifted index). Their radar structures were much weaker than any of the electrified categories. For example, on average their 30-dBZ echo barely penetrated above the freezing altitude (~4.5 km MSL during STEPS).

Overall, about 95% of no-lightning features had 40-dBZ echo below the altitude of −5°C (Fig. 7). For 30-dBZ echo, however, the corresponding temperature for this percentage was −30°C. Indeed, about half of all no-lightning features contained 30-dBZ echo above the freezing altitude. However, there was a flip side to this observation. About 30% of electrified features did not have 40-dBZ echo above the freezing altitude, while 90%–95% of them contained 30-dBZ echo above this level.

Combining the two populations and computing lightning probabilities based on radar structure leads to Table 3. For 30- and 40-dBZ echoes that reached at least to low altitudes/high temperatures, there was a base probability of about 45% for a feature to contain lightning—consistent with the population of no-lightning features composing 55% of the total population of 28 463 STEPS features. This was probably higher than would be expected if a true census of all convective cells were done, as the definition of a radar feature required at least some 30-dBZ echo to be present. Hence, very weak convective cells were not considered. Regardless, 30-dBZ echo at or above the −10°C level provided a 72.3% chance for a feature to be electrified, while a −20°C threshold for 30 dBZ led to an 82% chance. To get over 90% probability of lightning with 30 dBZ required it to reach about −35°C. However, just breaching the freezing level with 40 dBZ was enough to get nearly 90% chance for lightning, while the common threshold of 40 dBZ at or above the −10°C altitude (see section 1c) gave a 92.9% chance of lightning.

Volume of 40-dBZ echo above the freezing altitude also appeared to be a very strong predictor of lightning, as having over 2 grid points (>8 km^3) of +40 dBZ at temperatures below 0°C led to a 91.1% chance for a feature to be producing lightning, while having greater than 8 points (>32 km^3) led to a 95.2% probability. By contrast, reaching better than 90% probability with 30-dBZ echo above the freezing altitude required more

TABLE 3. Probability of a feature to contain lightning as a function of the minimum temperature altitude reached by its 30- or 40-dBZ contours. For example, if the 30-dBZ contour reached *at least* −10°C or higher in altitude, then there was a 72.3% chance the feature contained lightning.

Temperature (°C)	30-dBZ probability (%)	40-dBZ probability (%)
35	44.9	46.1
30	45.0	47.4
25	45.5	49.8
20	47.1	57.1
15	49.7	69.7
10	53.1	80.0
5	54.7	82.8
0	61.0	88.2
−5	66.9	90.7
−10	72.3	92.9
−15	77.3	94.5
−20	82.0	95.7
−25	86.2	97.1
−30	88.6	97.7
−35	91.7	98.9
−40	94.8	99.5
−45	96.6	99.6
−50	98.8	99.8
−55	99.5	99.9
−60	99.6	99.8
−65	100.0	100.0

than 40 grid points (>160 km^3), and more than 75 pixels of +30 dBZ were required for 95.1% probability (>300 km^3).

The results used to develop Table 3 can be inverted, to examine the probability that lightning did not exist in a feature given reflectivity thresholds falling below the altitudes of various temperatures. For example, if 30 dBZ did not extend to the freezing altitude, then there was an 88.5% chance the feature had no lightning, while the corresponding percentage for 40 dBZ was 76.3%.

e. Sensitivity studies

To ensure the validity of the results, some sensitivity tests were performed. As noted before, about one-third of +CG features occurred during only 3 days. These days were removed from the dataset, and then +CG and −CG feature environments were compared again. CAPE associated with +CG features still exceeded that of −CG ones by nearly 2: 1 (i.e., 1499.3 to 835.4 J kg^{-1}). The lifted index differences also were similar to before, −3.9 to −2.7. Warm-cloud depth was still slightly greater for +CG features, by ~160 m. Shear differences were reduced, with 3-km shear becoming 10.0–9.3 m s^{-1} for +CG and −CG features, respectively, while 6-km shear difference became 15.6–15.3 m s^{-1}. The precipitable water advantage for +CG features was maintained, 27.0–24.9 mm. Of all these variables, only the 6-km shear difference was no longer significant at 99% confidence.

A simplified matching process between features and their environments was employed, where the nearest RUC grid point to a feature's centroid was used to determine its environment. Results were very similar to the ones shown in Tables 1 and 2. In another sensitivity study, the requirements for number of active LMA stations (i.e., 9) and maximum distance between the LMA and feature centroids (125 km) were removed (features still had to fit within the limited confines of the 300 km × 300 km radar grid, of course). This increased total features by about 50%, but differences in instability, moisture, and shear between +CG and −CG features remained of similar magnitudes to those in Tables 1 and 2. In general, no matter what was done, the fundamental association of +CG features with significantly increased instability (50%–100% greater than −CG features), slightly increased shear and moisture, and slightly increased warm-cloud depth remained.

LMA sensitivity was studied by examining results only for radar features within 60 km of the LMA centroid. This was essentially within the physical confines of the LMA network (Thomas et al. 2004), where sensitivity was maximized. As noted in the discussion of Fig. 5, this quartered the size of the feature dataset, but average source rates for each feature type were within 10%–15% of the numbers in Table 1, and source rate differences between +CG and −CG features slightly increased (2984 vs 749 min^{-1}). No-CG features averaged 184 min^{-1}. Thus, using LMA source rates was a valid way of distinguishing electrical activity between different storms, even out to 125 km.

4. Discussion and conclusions

a. CLEAR

A framework for the statistical analysis of large radar and lightning datasets, called CLEAR, has been described and implemented in order to study two research problems in atmospheric electricity: +CG-dominated storms and estimating the probability of lightning using radar data. CLEAR is fully modular, allowing the inclusion or exclusion of a variety of datasets based on a study's objectives, including polarimetric and multiple-Doppler radar observations, 2D and 3D lightning mapping data, meteorological observations of storm environments, and other data. CLEAR involves the automated identification of radar features, or representations of convective storms. These features are linked, via various spatial and temporal criteria, to data on lightning and the meteorological environment. All of this information

is stored in modified NetCDF radar grids, allowing the rapid analysis of relationships between variables.

b. +CG storms

The results from the analysis of +CG-dominated features suggest that such cells were more electrically active, and contained midlevel positive charge (−10° to −30°C), in contrast to −CG-dominated cells that typically had positive charge at upper (near −40°C) and lower levels (0° to −10°C). The +CG features also had larger volumes and were more vertically developed compared to −CG features, similar to the results of Gilmore and Wicker (2002) and Lang and Rutledge (2002). This suggests the existence of strong, broad updrafts that could lead to large liquid water contents and positive charging of graupel at midlevels (Williams et al. 2005), thereby inverting the charge structure. These results are broadly consistent with the vast majority of recent research on +CG storm structure and evolution (Wiens et al. 2005; Kuhlman et al. 2006; Tessendorf et al. 2007a; MacGorman et al. 2008), but lend a considerable amount of statistical robustness that these past studies lacked, since they were often based on only 1–2 cases apiece.

The +CG features were associated with environments that were more conducive to intense convection—especially in terms of increased moisture, wind shear (Brook et al. 1982; Engholm et al. 1990), and instability—when compared to −CG features. Of these, the instability measures (e.g., CAPE and lifted index) were the most different between the storm types, often by 50%–100%. They also were the least sensitive to adjustments in analysis methodology. It is interesting that these basic measures of instability were so important in this study, given that Carey and Buffalo (2007) found no statistically significant relationship between them and +CG storms (though they did find such relationships for instability in select layers). However, the STEPS results support the instability predictions of Williams et al. (2005).

These differences in instability, coupled with the enhanced shear and moisture, likely explain why +CG features were so much larger and more intense, on average. However, there was not a specific threshold for individual environmental parameters, beyond which +CG storms were expected. This makes sense, since the RUC cannot be expected to provide a perfect sounding for every storm, nor is the environment the only possible control on the intensity of a storm. For example, cell mergers can lead to more intense storms and +CG activity (Carey et al. 2003a).

Interestingly, cloud-base height (and by extension warm-cloud depth) was not particularly different between +CG and −CG features. If anything, +CG features tended to have slightly deeper warm-cloud layers. This observation contrasted with the predictions of Williams et al. (2005), as well as the observations of Lang and Rutledge (2006) and Carey and Buffalo (2007). However, these results cannot necessarily be considered as a refutation of the warm-cloud hypothesis, as cloud base may become more important when considering separate geographical regions with distinct climatological environments.

The electrical analysis used decimated VHF source data out to 125-km range. Sensitivity studies supported this methodology, as very similar results were obtained for only short-range features, although activity within the lower positive charge layer of −CG features may have been better resolved closer to the LMA network. The utility of longer-range VHF sources in this study contrasts with the results of studies using other networks (Boccippio et al. 2001b; Carey et al. 2005; Ely et al. 2008).

c. Estimating lightning probability

CLEAR was also used to examine lightning probability for a spectrum of radar structures. Much past research (e.g., Buechler and Goodman 1990; Gremillion and Orville 1999; Vincent et al. 2003; Wolf 2007; Stano et al. 2010) was focused on finding the best radar predictor for lightning in terms of skill scores and lead time, limiting the application of their results in forensic meteorology. The present study utilized total lightning information to examine 12 790 lightning-producing features and 15 673 features with no lightning. Based on the results, the existence of 30-dBZ echo above the freezing altitude is a necessary condition (in ~90% of cases) for the occurrence of lightning, though not a sufficient one. The latter is fulfilled in ~90% of cases when 40-dBZ echo breaches the freezing altitude. In other words, of the two common reflectivity thresholds (30 and 40 dBZ), 40-dBZ echo altitude or volume was the superior estimator for the occurrence of lightning, while 30 dBZ was better for inferring the lack of lightning.

These results apply only to contemporaneous cell behavior, and no attempt was made to predict future lightning behavior based on current radar observations. In addition, these results may be specific to the STEPS region. Regardless, these results have implications for the issuance of lightning warnings (both for the occurrence and cessation of lightning), as well as for inferring the presence of lightning in forensic meteorology.

d. Limitations and future work

This paper presented only a fraction of the analysis capabilities of CLEAR. For example, features were not tracked in this study, thus excluding the possibility of examining storm evolution, cell mergers and splits, as well as inferring potential time-dependent relationships.

Radar grids were coarse, and care should be exercised when applying lightning probabilities to higher-resolution data. Polarimetric radar data and multiple-Doppler syntheses were not examined, thereby excluding information on the kinematic and microphysical structures of storms. Also, full-rate LMA data were not used and lightning flashes were not classified. VHF source distributions were examined only in the vertical, ignoring the horizontal heterogeneity that can exist in thunderstorm charge structures (Stolzenburg et al. 1998a,b,c, 2002; Lang and Rutledge 2008; Weiss et al. 2008). Data on the meteorological environments of features were obtained from forecast model analyses instead of soundings taken directly in the inflow of storms. Finally, aerosol data were not considered, despite the effects they can have on convection and lightning (Andreae et al. 2004; Lyons et al. 1998; Murray et al. 2000; Khain et al. 2005; Lang and Rutledge 2006; Rosenfeld et al. 2007; Wang et al. 2009).

An advantage of CLEAR is that it enables the comparison of a variety of datasets. Thus, STEPS results can be compared against those in other regions. In particular, future work will focus on combined observations in the vicinities of the Oklahoma, northern Alabama, and Washington, D.C., LMAs. As these regions demonstrate considerable differences in lightning behavior (Boccippio et al. 2001a; Orville and Huffines 2001), this will allow the analysis of regional controls on convection and lightning.

Acknowledgments. The authors are grateful to Paul Hein and Amanda Anderson for their assistance with development and testing of CLEAR. Some of the code for CLEAR was taken from the xlma software developed at New Mexico Tech, which also provided the LMA data. WSR-88D data were obtained from the National Climate Data Center. NLDN data were obtained from Vaisala, Inc. RUC data were obtained from the Department of Energy. This research was funded by the National Science Foundation via Grants ATM-0649034 and AGS-1010G6S7. The IDL code base for CLEAR is available upon request.

REFERENCES

Andreae, M. O., D. Rosenfeld, P. Artaxo, A. A. Costa, G. P. Frank, K. M. Longo, and M. A. F. Silva-Dias, 2004: Smoking rain clouds over the Amazon. *Science,* **303,** 1337–1342.

Benjamin, S. G., and Coauthors, 2004a: An hourly assimilation–forecast cycle: The RUC. *Mon. Wea. Rev.,* **132,** 495–518.

——, G. A. Grell, J. M. Brown, T. G. Smirnova, and R. Bleck, 2004b: Mesoscale weather prediction with the RUC hybrid isentropic–terrain-following coordinate model. *Mon. Wea. Rev.,* **132,** 473–494.

Boccippio, D. J., K. L. Cummins, H. J. Christian, and S. J. Goodman, 2001a: Combined satellite- and surface-based estimation of the intracloud–cloud-to-ground lightning ratio over the continental United States. *Mon. Wea. Rev.,* **129,** 108–122.

——, S. Heckman, and S. J. Goodman, 2001b: A diagnostic analysis of the Kennedy Space Center LDAR network 1. Data characteristics. *J. Geophys. Res.,* **106,** 4769–4786.

Branick, M. L., and C. A. Doswell III, 1992: An observation of the relationship between supercell structure and lightning ground strike polarity. *Wea. Forecasting,* **7,** 143–149.

Brook, M., M. Nakano, P. Krehbiel, and T. Takeuti, 1982: The electrical structure of the 23 Hokuriku winter thunderstorms. *J. Geophys. Res.,* **87** (C2), 1207–1215.

Buechler, D. E., and S. J. Goodman, 1990: Echo size and asymmetry: Impact on NEXRAD storm identification. *J. Appl. Meteor.,* **29,** 962–969.

Carey, L. D., and S. A. Rutledge, 1996: A multiparameter radar case study of the microphysical and kinematic evolution of a lightning producing storm. *Meteor. Atmos. Phys.,* **59,** 33–64.

——, and ——, 1998: Electrical and multiparameter radar observations of a severe hailstorm. *J. Geophys. Res.,* **103,** 13 979–14 000.

——, and ——, 2003: Characteristics of cloud-to-ground lightning in severe and nonsevere storms over the central United States from 1989–1998. *J. Geophys. Res.,* **108,** 4483, doi:10.1029/2002JD002951.

——, and K. M. Buffalo, 2007: Environmental control of cloud-to-ground lightning polarity in severe storms. *Mon. Wea. Rev.,* **135,** 1327–1353.

——, W. A. Petersen, and S. A. Rutledge, 2003a: Evolution of cloud-to-ground lightning and storm structure in the Spencer, South Dakota, tornadic supercell of 30 May 1998. *Mon. Wea. Rev.,* **131,** 1811–1831.

——, S. A. Rutledge, and W. A. Petersen, 2003b: The relationship between severe storm reports and cloud-to-ground lightning in the contiguous United States from 1989 to 1998. *Mon. Wea. Rev.,* **131,** 1211–1228.

——, M. J. Murphy, T. L. McCormick, and N. W. S. Demetriades, 2005: Lightning location relative to storm structure in a leading-line, trailing-stratiform mesoscale convective system. *J. Geophys. Res.,* **110,** D03105, doi:10.1029/2003JD004371.

Christian, H. J., 2008: The Geostationary Lightning Mapper Instrument for GOES-R. Preprints, *Third Conf. on Meteorological Applications of Lightning Data*, New Orleans, LA, Amer. Meteor. Soc., 3.4. [Available online at http://ams.confex.com/ams/88Annual/techprogram/paper_139468.htm.]

——, R. J. Blakeslee, and S. J. Goodman, 1989: The detection of lightning from geostationary orbit. *J. Geophys. Res.,* **94** (D11), 13 329–13 337.

Cressman, G. P., 1959: An operational objective analysis system. *Mon. Wea. Rev.,* **87,** 367–374.

Cummins, K. L., and M. J. Murphy, 2009: An overview of lightning locating systems: History, techniques, and data uses, with an in-depth look at the U.S. NLDN. *IEEE Trans. Electromagn. Compat.,* **51,** 499–518, doi:10.1109/TEMC.2009.2023450.

——, ——, E. A. Bardo, W. L. Hiscox, R. B. Pyle, and A. E. Pifer, 1998: A combined TOA/MDF technology upgrade of the U. S. National Lightning Detection Network. *J. Geophys. Res.,* **103,** 9035–9044.

Curran, E. B., and W. D. Rust, 1992: Positive ground flashes produced by low-precipitation thunderstorms in Oklahoma on 26 April 1984. *Mon. Wea. Rev.,* **120,** 544–553.

Deierling, W., and W. A. Petersen, 2008: Total lightning activity as an indicator of updraft characteristics. *J. Geophys. Res.,* **113,** D16210, doi:10.1029/2007JD009598.

——, ——, J. Latham, S. Ellis, and H. J. Christian, 2008: The relationship between lightning activity and ice fluxes in thunderstorms. *J. Geophys. Res.,* **113,** D15210, doi:10.1029/2007JD009700.

Dixon, M., and G. Wiener, 1993: TITAN: Thunderstorm Identification, Tracking, Analysis, and Nowcasting—A radar-based methodology. *J. Atmos. Oceanic Technol.,* **10,** 785–797.

Dye, J. E., W. P. Winn, J. J. Jones, and D. W. Breed, 1989: The electrification of New Mexico thunderstorms. 1. Relationship between precipitation development and the onset of electrification. *J. Geophys. Res.,* **94,** 8643–8656.

Ely, B. L., R. E. Orville, L. D. Carey, and C. L. Hodapp, 2008: Evolution of the total lightning structure in a leading-line, trailing-stratiform mesoscale convective system over Houston, Texas. *J. Geophys. Res.,* **113,** D08114, doi:10.1029/2007JD008445.

Engholm, C. D., E. R. Williams, and R. M. Dole, 1990: Meteorological and electrical conditions associated with positive cloud-to-ground lightning. *Mon. Wea. Rev.,* **118,** 470–487.

Gauthier, M. L., W. A. Petersen, and L. D. Carey, 2010: Cell mergers and their impact on cloud-to-ground lightning over the Houston area. *Atmos. Res.,* **96,** 626–632.

Gilmore, M. S., and L. J. Wicker, 2002: Influences of the local environment on supercell cloud-to-ground lightning, radar characteristics, and severe weather on 2 June 1995. *Mon. Wea. Rev.,* **130,** 2349–2372.

Goodman, S. J., D. E. Buechler, P. D. Wright, and W. D. Rust, 1988: Lightning and precipitation history of a microburst-producing storm. *Geophys. Res. Lett.,* **15,** 1185–1188.

Gremillion, M. S., and R. E. Orville, 1999: Thunderstorm characteristics of cloud-to-ground at the Kennedy Space Center, Florida: A study of lightning initiation signatures as indicated by the WSR-88D. *Wea. Forecasting,* **14,** 640–649.

Hane, C. E., J. A. Haynes, D. L. Andra, and F. H. Carr, 2008: The evolution of morning convective systems over the U.S. Great Plains during the warm season. Part II: A climatology and the influence of environmental factors. *Mon. Wea. Rev.,* **136,** 929–944.

Johnson, J. T., P. L. MacKeen, A. Witt, E. D. Mitchell, G. J. Stumpf, M. D. Eilts, and K. W. Thomas, 1998: The storm cell identification and tracking algorithm: An enhanced WSR-88D algorithm. *Wea. Forecasting,* **13,** 263–276.

Kalb, C. P., 2007: Cloud-to-ground lightning polarity and environmental conditions over the central United States. M.S. thesis, Department of Atmospheric Science, Colorado State University, 123 pp.

Khain, A., D. Rosenfeld, and A. Pokrovsky, 2005: Aerosol impact on the dynamics and microphysics of deep convective clouds. *Quart. J. Roy. Meteor. Soc.,* **131,** 2639–2663.

Krehbiel, P. R., J. A. Riousset, V. P. Pasko, R. J. Thomas, W. Rison, M. A. Stanley, and H. E. Edens, 2008: Upward electrical discharges from thunderstorms. *Nat. Geosci.,* **1,** 233–237.

Kuhlman, K. M., C. L. Ziegler, E. R. Mansell, D. R. MacGorman, and J. M. Straka, 2006: Numerically simulated electrification and lightning of the 29 June 2000 STEPS supercell storm. *Mon. Wea. Rev.,* **134,** 2734–2757.

Lang, T. J., and S. A. Rutledge, 2002: Relationships between convective storm kinematics, precipitation, and lightning. *Mon. Wea. Rev.,* **130,** 2492–2506.

——, and ——, 2006: Cloud-to-ground lightning downwind of the 2002 Hayman forest fire in Colorado. *Geophys. Res. Lett.,* **33,** L03804, doi:10.1029/2005GL024608.

——, and ——, 2008: Kinematic, microphysical, and electrical aspects of an asymmetric bow-echo mesoscale convective system observed during STEPS 2000. *J. Geophys. Res.,* **113,** D08213, doi:10.1029/2006JD007709.

——, ——, J. E. Dye, M. Venticinque, P. Laroche, and E. Defer, 2000: Anomalously low negative cloud-to-ground lightning flash rates in intense convective storms observed during STERAO-A. *Mon. Wea. Rev.,* **128,** 160–173.

——, and Coauthors, 2004a: The Severe Thunderstorm Electrification and Precipitation Study (STEPS). *Bull. Amer. Meteor. Soc.,* **85,** 1107–1125.

——, S. A. Rutledge, and K. C. Wiens, 2004b: Origins of positive cloud-to-ground lightning flashes in the stratiform region of a mesoscale convective system. *Geophys. Res. Lett.,* **31,** L10105, doi:10.1029/2004GL019823.

——, W. A. Lyons, S. A. Rutledge, J. D. Meyer, D. R. MacGorman, and S. A. Cummer, 2010: Transient luminous events above two mesoscale convective systems: Storm structure and evolution. *J. Geophys. Res.,* **115,** A00E22, doi:10.1029/2009JA014500.

Larsen, H. R., and E. J. Stansbury, 1974: Association of lightning flashes with precipitation cores extending to height 7 km. *J. Atmos. Terr. Phys.,* **36,** 1547–1553.

Lay, E. H., R. H. Holzworth, C. J. Rodger, J. N. Thomas, O. Pinto, and R. L. Dowden, 2004: WWLL global lightning detection system: Regional validation study in Brazil. *Geophys. Res. Lett.,* **31,** L03102, doi:10.1029/2003GL018882.

Lyons, W. A., T. E. Nelson, E. R. Williams, J. A. Cramer, and T. R. Turner, 1998: Enhanced positive cloud-to-ground lightning in thunderstorms ingesting smoke from fires. *Science,* **282,** 77–80.

——, ——, R. A. Armstrong, V. P. Pasko, and M. A. Stanley, 2003a: Upward electrical discharges from thunderstorm tops. *Bull. Amer. Meteor. Soc.,* **84,** 445–454.

——, ——, E. R. Williams, S. A. Cummer, and M. A. Stanley, 2003b: Characteristics of sprite-producing positive cloud-to-ground lightning during the 19 July 2000 STEPS mesoscale convective systems. *Mon. Wea. Rev.,* **131,** 2417–2427.

——, S. A. Cummer, M. A. Stanley, G. R. Huffines, K. C. Wiens, and T. E. Nelson, 2008: Supercells and sprites. *Bull. Amer. Meteor. Soc.,* **89,** 1165–1174.

MacGorman, D. R., and D. W. Burgess, 1994: Positive cloud-to-ground lightning in tornadic storms and hailstorms. *Mon. Wea. Rev.,* **122,** 1671–1697.

——, ——, V. Mazur, W. D. Rust, W. L. Taylor, and B. C. Johnson, 1989: Lightning rates relative to tornadic storm evolution on 22 May 1981. *J. Atmos. Sci.,* **46,** 221–250.

——, W. D. Rust, P. Krehbiel, W. Rison, E. Bruning, and K. Wiens, 2005: The electrical structure of two supercell storms during STEPS. *Mon. Wea. Rev.,* **133,** 2583–2607.

——, and Coauthors, 2008: TELEX The Thunderstorm Electrification and Lightning Experiment. *Bull. Amer. Meteor. Soc.,* **89,** 997–1013.

Mansell, E. R., D. R. MacGorman, C. Ziegler, and J. M. Straka, 2002: Simulated three-dimensional branched lightning in a numerical thunderstorm model. *J. Geophys. Res.,* **107,** 4075, doi:10.1029/2000JD000244.

——, ——, C. L. Ziegler, and J. M. Straka, 2005: Charge structure and lightning sensitivity in a simulated multicell thunderstorm. *J. Geophys. Res.,* **110,** D12101, doi:10.1029/2004JD005287.

Markowski, P., C. Hannon, J. Frame, E. Lancaster, A. Pietrycha, R. Edwards, and R. L. Thompson, 2003: Characteristics of vertical wind profiles near supercells obtained from the rapid update cycle. *Wea. Forecasting,* **18,** 1262–1272.

Marshall, J. S., and S. Radhakant, 1978: Radar precipitation maps as lightning indicators. *J. Appl. Meteor.,* **17,** 206–212.

McCaul, E. W., D. E. Buechler, S. Hodanish, and S. J. Goodman, 2002: The Almena, Kansas, tornadic storm of 3 June 1999: A long-lived supercell with very little cloud-to-ground lightning. *Mon. Wea. Rev.,* **130,** 407–415.

Michimoto, K., 1991: A study of radar echoes and their relation to lightning discharge of thunderclouds in the Hokuriku District. Part I: Observation and analysis of thunderclouds in summer and winter. *J. Meteor. Soc. Japan,* **69,** 327–335.

——, 1993: A study of radar echoes and their relation to lightning discharge of thunderclouds in the Hokuriku District. Part II: Observation and analysis of ''single flash'' thunderclouds in midwinter. *J. Meteor. Soc. Japan,* **71,** 195–204.

Murray, N. D., R. E. Orville, and G. R. Huffines, 2000: Effect of pollution from Central American fires on cloud-to-ground lightning in May 1998. *Geophys. Res. Lett.,* **27,** 2249–2252.

Neilley, P. P., and R. B. Bent, 2009: An overview of the United States Precision Lightning Network (USPLN). Preprints, *Fourth Conf. on the Meteorological Applications of Lightning Data,* Phoenix, AZ, Amer. Meteor. Soc., 4.2. [Available online at http://ams.confex.com/ams/89annual/techprogram/paper_149149.htm.]

Orville, R. E., and G. R. Huffines, 2001: Cloud-to-ground lightning in the United States: NLDN results in the first decade, 1989–98. *Mon. Wea. Rev.,* **129,** 1179–1193.

Petersen, W. A., S. A. Rutledge, and R. E. Orville, 1996: Cloud-to-ground lightning observations from TOGA COARE: Selected results and lightning location algorithms. *Mon. Wea. Rev.,* **124,** 602–620.

Potvin, C. K., K. L. Elmore, and S. J. Weiss, 2010: Assessing the impacts of proximity sounding criteria on the climatology of significant tornado environments. *Wea. Forecasting,* **25,** 921–930.

Reap, R. M., and D. R. MacGorman, 1989: Cloud-to-ground lightning: Climatological characteristics and relationships to model fields, radar observations, and severe local storms. *Mon. Wea. Rev.,* **117,** 518–535.

Rison, W., R. J. Thomas, P. R. Krehbiel, T. Hamlin, and J. Harlin, 1999: A GPS-based three-dimensional lightning mapping system: Initial observations in central New Mexico. *Geophys. Res. Lett.,* **26,** 3573–3576.

Rosenfeld, D., M. Fromm, J. Trentmann, G. Luderer, M. O. Andreae, and R. Servranckx, 2007: The Chisholm firestorms: Observed microstructure, precipitation, and lightning activity of a pyro-cumulonimbus. *Atmos. Chem. Phys.,* **7,** 645–659.

Rowe, A. K., S. A. Rutledge, and T. J. Lang, 2011: Investigation of microphysical processes occurring in isolated convection during NAME. *Mon. Wea. Rev.,* **139,** 424–443.

Rust, W. D., and D. R. MacGorman, 2002: Possibly inverted-polarity electrical structures in thunderstorms during STEPS. *Geophys. Res. Lett.,* **29,** 1571, doi:10.1029/2001GL014303.

——, and Coauthors, 2005: Inverted-polarity electrical structures in thunderstorms in the Severe Thunderstorm Electrification and Precipitation Study (STEPS). *Atmos. Res.,* **76,** 247–271, doi:10.1016/j.atmosres.2004.11.029.

Ryzhkov, A. V., T. J. Schuur, D. W. Burgess, P. L. Heinselman, S. E. Giangrande, and D. S. Zrnic, 2005: The Joint Polarization Experiment: Polarimetric rainfall measurements and hydrometeor classification. *Bull. Amer. Meteor. Soc.,* **86,** 809–824.

Saunders, C. P. R., and S. L. Peck, 1998: Laboratory studies of the influence of the rime accretion rate on charge transfer during graupel/crystal collisions. *J. Geophys. Res.,* **103,** 13 949–13 956.

——, W. D. Keith, and R. P. Mitzeva, 1991: The effect of liquid water on thunderstorm charging. *J. Geophys. Res.,* **96,** 11 007–11 017.

Schumacher, R. S., and R. H. Johnson, 2005: Organization and environmental properties of extreme-rain-producing mesoscale convective systems. *Mon. Wea. Rev.,* **133,** 961–976.

Seimon, A., 1993: Anomalous cloud-to-ground lightning in an F5 tornado-producing supercell thunderstorm on 28 August 1990. *Bull. Amer. Meteor. Soc.,* **74,** 189–203.

Smith, S. B., J. G. LaDue, and D. R. MacGorman, 2000: The relationship between cloud-to-ground polarity and surface equivalent potential temperature during three tornadic outbreaks. *Mon. Wea. Rev.,* **128,** 3320–3328.

Stano, G. T., H. E. Fuelberg, and W. P. Roeder, 2010: Developing empirical lightning cessation forecast guidance for the Cape Canaveral Air Force Station and Kennedy Space Center. *J. Geophys. Res.,* **115,** D09205, doi:10.1029/2009JD013034.

Stolzenburg, M., 1994: Observations of high ground flash densities of positive lightning in summertime thunderstorms. *Mon. Wea. Rev.,* **122,** 1740–1750.

——, W. D. Rust, B. F. Smull, and T. C. Marshall, 1998a: Electrical structure in thunderstorm convective regions. Part I: Mesoscale convective systems. *J. Geophys. Res.,* **103,** 14 059–14 078.

——, ——, and T. C. Marshall, 1998b: Electrical structure in thunderstorm convective regions. Part II: Isolated storms. *J. Geophys. Res.,* **103,** 14 079–14 096.

——, ——, and ——, 1998c: Electrical structure in thunderstorm convective regions. Part III: Synthesis. *J. Geophys. Res.,* **103,** 14 097–14 108.

——, T. C. Marshall, W. D. Rust, and D. L. Bartels, 2002: Two simultaneous charge structures in thunderstorm convection. *J. Geophys. Res.,* **107,** 4352, doi:10.1029/2001JD000904.

Stuhlmann, R., A. Rodriguez, S. Tjemkes, J. Grandell, A. Arriaga, J. Bézy, D. Aminou, and P. Bensi, 2005: Plans for EUMETSAT's Third Generation Meteosat geostationary satellite programme. *Adv. Space Res.,* **36,** 975–981.

Takahashi, T., 1978: Riming electrification as a charge generation mechanism in thunderstorms. *J. Atmos. Sci.,* **35,** 1536–1548.

Tessendorf, S. A., L. J. Miller, K. C. Wiens, and S. A. Rutledge, 2005: The 29 June 2000 supercell observed during STEPS. Part I: Kinematics and microphysics. *J. Atmos. Sci.,* **62,** 4127–4150.

——, S. A. Rutledge, and K. C. Wiens, 2007a: Radar and lightning observations of normal and inverted polarity multicellular storms from STEPS. *Mon. Wea. Rev.,* **135,** 3682–3706.

——, K. C. Wiens, and S. A. Rutledge, 2007b: Radar and lightning observations of the 3 June 2000 electrically inverted storm from STEPS. *Mon. Wea. Rev.,* **135,** 3665–3681.

Thomas, R. J., P. R. Krehbiel, W. Rison, S. J. Hunyady, W. P. Winn, T. Hamlin, and J. Harlin, 2004: Accuracy of the Lightning Mapping Array. *J. Geophys. Res.,* **109,** D14207, doi:10.1029/2004JD004549.

Thompson, R. L., R. Edwards, J. A. Hart, K. L. Elmore, and P. Markowski, 2003: Close proximity soundings within supercell environments obtained from the rapid update cycle. *Wea. Forecasting,* **18,** 1243–1261.

Vincent, B. R., L. D. Carey, D. Schneider, K. Keeter, and R. Gonski, 2003: Using WSR-88D reflectivity data for the prediction of cloud-to-ground lightning: A North Carolina study. *Natl. Wea. Dig.,* **27,** 35–44.

Walpole, R. E., R. H. Meyers, S. L. Myers, and K. Ye, 2002: *Probability and Statistics for Scientists and Engineers*. 7th ed. Prentice Hall, 730 pp.

Wang, J., S. C. van den Heever, and J. S. Reid, 2009: A conceptual model for the link between Central American biomass burning

aerosols and severe weather over the south central United States. *Environ. Res. Lett.,* **4,** 015003, doi:10.1088/1748-9326/4/1/015003.

Warner, T. A., J. H. Helsdon Jr., and A. G. Detwiler, 2003: Aircraft observations of a lightning channel in STEPS. *Geophys. Res. Lett.,* **30,** 1984, doi:10.1029/2003GL017334.

Weiss, S. A., W. D. Rust, D. R. MacGorman, E. C. Bruning, and P. R. Krehbiel, 2008: Evolving complex electrical structures of the STEPS 25 June 2000 multicell storm. *Mon. Wea. Rev.,* **136,** 741–756.

Wiens, K. C., S. A. Rutledge, and S. A. Tessendorf, 2005: The 29 June 2000 supercell observed during STEPS. Part II: Lightning and charge structure. *J. Atmos. Sci.,* **62,** 4151–4177.

Williams, E. R., 1989: The tripole structure of thunderstorms. *J. Geophys. Res.,* **94,** 13 151–13 167.

——, 2001: The electrification of severe storms. *Severe Convective Storms, Meteor. Monogr.,* No. 50, Amer. Meteor. Soc., 527–561.

——, V. Mushtak, D. Rosenfeld, S. Goodman, and D. Boccippio, 2005: Thermodynamic conditions favorable to superlative thunderstorm updraft, mixed phase microphysics and lightning flash rate. *Atmos. Res.,* **76,** 288–306.

Wolf, P., 2007: Anticipating the initiation, cessation, and frequency of cloud-to-ground lightning, utilizing WSR-88D reflectivity data. *Electron. J. Operat. Meteor.,* 2007-EJ1. [Available online at http://www.nwas.org/ej/2007-EJ1/.]

Workman, E. J., and S. E. Reynolds, 1949: Electrical activity as related to thunderstorm cell growth. *Bull. Amer. Meteor. Soc.,* **30,** 142–144.

Zajac, B. A., and S. A. Rutledge, 2001: Cloud-to-ground lightning activity in the contiguous United States from 1995 to 1999. *Mon. Wea. Rev.,* **129,** 999–1019.